Journal of Materials Chemistry B

PAPER

View Article Online
View Journal | View Issue

Cite this: J. Mater. Chem. B, 2014, 2, 2733

An intercompartmental enzymatic cascade reaction in channel-equipped polymersome-in-polymersome architectures†

Winna Siti,‡[a] Hans-Peter M. de Hoog,‡[b] Ozana Fischer,[c] Wong Yee Shan,[d] Nikodem Tomczak,[b] Madhavan Nallani*[a] and Bo Liedberg[a]

Received 27th December 2013
Accepted 27th February 2014

DOI: 10.1039/c3tb21849j

www.rsc.org/MaterialsB

Compartmentalization, as a design principle, is a prerequisite for the functioning of eukaryotic cells. Although cell mimics in the form of single vesicular compartments such as liposomes or polymersomes have been tremendously successful, investigations of the corresponding higher-order architectures, in particular bilayer-based multicompartment vesicles, have only recently gained attention. We hereby demonstrate a multicompartment cell-mimetic nanocontainer, built-up from fully synthetic membranes, which features an inner compartment equipped with a channel protein and a semi-permeable outer compartment that allows passive diffusion of small molecules. The functionality of this multicompartment architecture is demonstrated by a cascade reaction between enzymes that are segregated in separate compartments. The unique architecture of polymersomes, which combines stability with a cell-membrane-mimetic environment, and their assembly into higher-order architectures could serve as a design principle for new generation drug-delivery vehicles, biosensors, and protocell models.

Introduction

Compartmentalization is the key organizational feature of eukaryotic cells, providing organelles that perform vital cellular functions such as protein synthesis, selective degradation and energy generation.[1,2] It is quite remarkable that the construction of soft matter multicompartment architectures with functional properties has received comparatively limited attention. Only a handful of reports on functional multicompartment structures exist to date,[3–13] while the number of studies on single vesicles is immense. A prototypical example of a multicompartment vesicular structure based on amphiphilic self-assembly was reported by Bolinger *et al.*, who prepared surface-immobilized vesicle-in-vesicle architectures, and demonstrated temperature-controlled mixing of the vesicle's contents.[14] Such 'vesosomes' exhibit interesting controlled-release properties.[15,16] The limited number of reports on multicompartment liposomes appears to stem primarily from the physicochemical and mechanical properties of these architectures, in particular the fluidity and the transient nature of the lipidic membranes, which leads to fusion and destabilization of the multicompartment structure.[17] Because of these shortcomings, researchers have developed synthetic, polymer-based, vesicle-like structures, such as polymersomes or layer-by-layer capsules, and used them to encapsulate enzymes or proteins.[18–21] Because of the structural stability of polymers, such capsules have been found to be well-suited for hosting enzymes, allowing cascade reactions,[22] and the embedment of membrane proteins such as porins.[23–27] They furthermore allow the fabrication of multicompartment structures.[5,6,10–13,28–30]

The control over permeability in multicompartment architectures has so far been based on the properties of the membrane itself. In contrast, the permeability of natural membranes is controlled by membrane proteins, which can exist either as passive channels or as highly selective pores (*e.g.*, ligand or ion gated) that facilitate the transport of molecules across the amphiphilic membrane. Indeed, the incorporation of membrane proteins would allow researchers to tap into the richness of membrane transport phenomena found in nature. Their integration into a multicompartment architecture represents a more complete mimic of cellular organization. In this respect, polymersomes are unique in that they contain a truly biomimetic amphiphilic bilayer membrane, which has been

[a]Centre for Biomimetic Sensor Science, School of Materials Science and Engineering, Nanyang Technological University, 50 Nanyang Drive 637553, Singapore. E-mail: MNallani@ntu.edu.sg

[b]Institute of Materials Research and Engineering, A*STAR (Agency for Science, Technology and Research), 3 Research Link 117602, Singapore

[c]University of Basel, Department of Chemistry, Klingelbergstrasse 80, Basel 4056, Switzerland

[d]School of Materials Science and Engineering, Nanyang Technological University, Block N4.1, Nanyang Avenue 639798, Singapore

† Electronic supplementary information (ESI) available: Experimental details, light scattering data, TEM images, scanning confocal images and flow cytometry data. See DOI: 10.1039/c3tb21849j

‡ Both authors contributed equally.

proven to allow the stable and functional immobilization of membrane proteins.[24,25,27,31–34] We demonstrate herein a multicompartment cell-mimetic architecture built from fully synthetic polymeric membranes, featuring a channel-equipped inner compartment and a semi-permeable outer compartment (Scheme 1). The functionality of the architecture is demonstrated by a cascade reaction between enzymes accommodated in the separate compartments.

We have previously demonstrated the selective compartmentalization of different biomacromolecules in multicompartment polymersomes (hereafter termed MCPs).[28] These MCPs were generated in high yield (50% of the possible architectures were MCPs) and displayed dimensions in the submicron range, making them potentially suitable for *in vivo* applications.[7] The design of the current system is outlined in Scheme 1 and shows an inner compartment formed from ABA polymersomes (*i.e.*, $PMOXA_{12}$–$PDMS_{55}$–$PMOXA_{12}$: poly(2-methyloxazoline)–poly(dimethylsiloxane)–poly(2-methyloxazoline)), which encapsulates the enzyme horseradish peroxidase (HRP). Importantly, outer-membrane protein F (OmpF), a passive diffusion channel that allows the passage of small molecules and ions, is inserted in the ABA membrane. The ABA vesicles are encapsulated, along with the enzyme glucose oxidase (GOx), into PS–PIAT (*i.e.*, polystyrene–poly(L-isocyanoalanine(2-thiophen-3-yl-ethyl)amide)) polymersomes. PS–PIAT membranes are known to be semi-permeable and to allow the diffusion of small organic molecules.[35] The cascade reaction described herein is therefore facilitated by diffusion through the semi-permeable membrane of the outer compartment, and subsequently, through the channels provided by OmpF inserted in the inner compartment's membrane. To demonstrate the proof of concept, we selected a common bienzymatic reaction used for the colorimetric determination of glucose, where GOx catalyzes the oxidation of β-D-glucose to produce D-gluconolactone and H_2O_2. H_2O_2 acts as a co-substrate for the HRP catalyzed oxidation of amplex red (10-acetyl-3,7-dihydroxyphenoxazine) to the fluorescent resorufin (Scheme 1a).

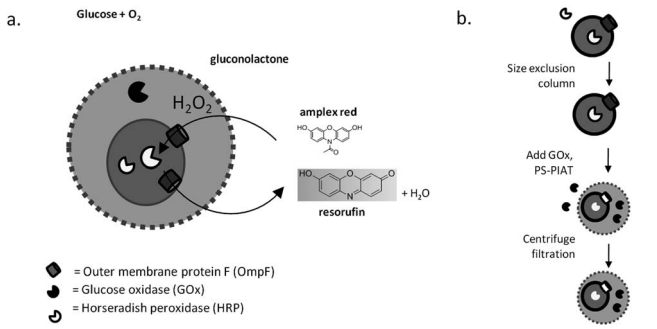

Scheme 1 (a) Design of enzymatically active multicompartment polymersomes (MCPs): the porin OmpF is embedded in the inner compartment's tri-block copolymer membrane, which itself is encapsulated in a larger semi-permeable polymersome. The structure facilitates a cascade reaction between the separately encapsulated enzymes horseradish peroxidase (HRP) and glucose oxidase (GOx). Hydrogen peroxide (H_2O_2) is generated by the oxidation of β-D-glucose and subsequently used in the catalytic oxidation of amplex red to the fluorescent end-product resorufin (shown in red). (b) Preparation procedure of the MCPs: the steps involve preparation of the inner 'channel-equipped' ABA polymersomes, carrying HRP, followed by encapsulation in PS–PIAT "outer" polymersomes, along with GOx.

Results and discussion

The ABA polymersomes, encapsulating HRP and with OmpF embedded in the membrane, were prepared as reported previously, leading to catalytically active nanocontainers (Fig. 1a, 2a and ESI S1†).[25–27] According to dynamic light scattering (DLS; Fig. 1d–e), the ABA polymer formed vesicles of *ca.* 90 nm in diameter. The diameter obtained from transmission electron microscopy (TEM) appeared to be in the range of 30–70 nm (for additional images, see Fig. S2†). Both TEM images and DLS data are in good agreement with reported values for ABA polymersomes.[36–38]

Multicompartment polymersomes were then prepared by dilution of the ABA polymersomes in a solution containing GOx, and subsequent addition of PS–PIAT. It was verified by light scattering and TEM that addition of tetrahydrofuran (THF) did not lead to disintegration of the ABA nanoreactors (Fig. S2 and S3†). ABA polymersomes encapsulating HRP (without OmpF) were prepared using the same procedure. The non-encapsulated GOx enzyme was removed by centrifugal filtration, and the enzymatic activity of the filtrates (or "flow-throughs") was measured to ensure no residual activity from the non-encapsulated enzyme (Fig. S4†).

TEM imaging of the MCPs showed the existence of empty PS–PIAT or ABA polymersomes (data not shown), as well as vesicles containing ABA polymersomes (Fig. 1c). From TEM imaging, it appeared that a number of ABA polymersomes were 'sticking' to the outer surface of the MCPs. We suggest this could be due to a drying effect during sample preparation for TEM imaging. In order to verify this hypothesis, we further attempted imaging of the internal structure of the MCPs by cryo-TEM (Fig. S2†). Despite the very low contrast of the internal

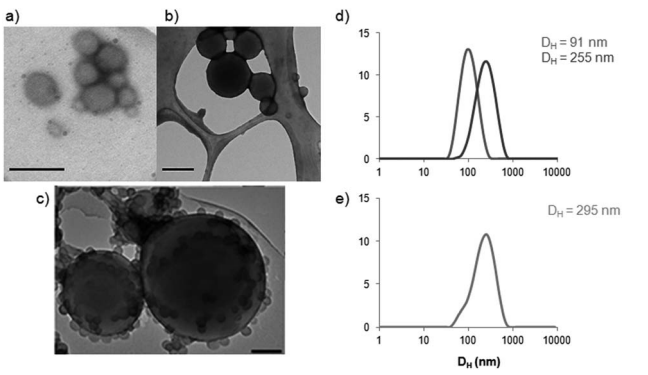

Fig. 1 Characterization of the MCPs. Representative TEM images of (a) ABA polymersomes, (b) PS–PIAT polymersomes, and (c) MCPs. In contrast to single PS–PIAT polymersomes, the MCP sample shows many small spherical vesicles within PS–PIAT polymersomes. (d) Hydrodynamic diameters (D_H) of individual ABA (red trace) and PS–PIAT polymersomes (blue trace) and (e) MCPs, showing the increased dimensions of the multicompartment structure. For (a) and (c), scale bars are 100 nm, for (b), scale bar is 200 nm.

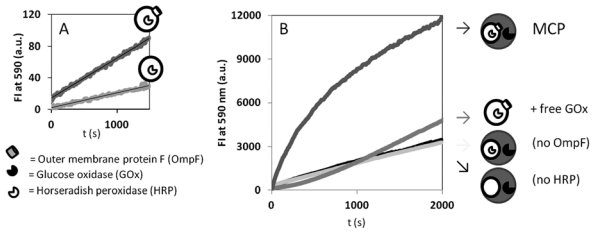

Fig. 2 Enzyme activity inside MCPs. (a) Conversion of amplex red by purified single ABA nanoreactors, with and without OmpF embedded in the membrane. (b) Cascade activity of the MCPs, showing an increased conversion of amplex red as compared to the controls. The identity of the samples is indicated schematically alongside the graph.

ABA polymersomes, no ABA polymersomes were found to be absorbed on the MCP surface (Fig. S2†). DLS data showed an increase in the hydrodynamic diameter (D_H) from 50–100 nm, for individual ABA polymersomes (Fig. 1d), to 295 nm for the multicompartments (Fig. 1e). Since PS–PIAT polymersomes alone showed a diameter of *ca.* 250 nm, the DLS results indicate that a unique population of polymersomes was formed. Static light scattering measurements of the MCPs provided a radius of gyration of 163 nm (±28), resulting in a R_G/R_H (ρ-value) of 1.10, indicative of the vesicular structure (Fig. S5†).[39] Because light scattering cannot readily distinguish between the multiple species of polymersomes that could be expected to be present in the MCP sample (*i.e.*, single PS–PIAT and ABA polymersomes, apart from MCPs), we also analyzed the MCPs using fluorescence microscopy and flow cytometry (see below).

To investigate the enzymatic activity of the MCPs, β-D-glucose and amplex red were added to the multicompartment polymersomes, which led to the rapid synthesis of the fluorescent product (Fig. 2b). This activity was compared to control experiments where no OmpF was present in the membrane, and single ABA nanoreactors in the presence of bulk GOx, as well as to a series of measurements for enzymes in the bulk solution. For bulk measurements, we fixed the concentration of GOx at 0.3 mg mL^{-1}, which was based on the GOx encapsulation efficiency (ee) (*ca.* 38%, as estimated by the measurement of dye-labeled GOx, before and after encapsulation, see Fig. S6 and Table S1† for details), while the concentration of HRP was varied between 10 μg mL^{-1} (the theoretical HRP concentration at 100% ee) and 40 ng mL^{-1} (ee: 0.4%). It was observed that the rate of amplex red formation increased with increasing HRP concentration (Fig. S8a†), which is especially clear when the initial rate of the reaction (v_0; approximating zero-order reaction kinetics) is plotted *versus* HRP concentration (Fig. S8b†). This revealed that, at concentrations below 5 μg mL^{-1}, HRP catalysis was the rate limiting factor (*i.e.*, above this concentration the initial rate did not increase linearly).

Comparison of the cascade activity of the MCPs revealed that the initial rate (v_0) of amplex red formation was significantly higher for the MCPs ($v_0 = 19.3$ au s^{-1}) than for the controls that contained no OmpF ($v_0 = 1.8$ au s^{-1}) or no HRP ($v_0 = 1.8$ au s^{-1}). Considering that HRP is the rate limiting factor in the cascade reaction, the close proximity of HRP and GOx allows for an enhanced conversion of amplex red, provided OmpF is present to facilitate diffusion of reactants.[40] Here it should be noted that diffusion of substrates into PS–PIAT is not limited to a great extent by the presence of the membrane if k_{cat} values are below 1000 s^{-1}.[41,42] The rate observed for the MCPs without OmpF was comparable to the MCPs without HRP ($v_0 = 1.8$ au s^{-1}) suggesting this activity to stem mainly from auto-oxidation of amplex red by the generated hydrogen peroxide. Auto-oxidation also contributed to a significant extent to the system containing 0.3 mg mL^{-1} free GOx and the single ABA nanoreactors, roughly containing the same enzyme concentrations as the multicompartment system. The eventual product yield (at $t = 2000$ s), as judged from the fluorescence intensity, was, however, at least a factor of 2 higher than that for the MCP control reaction, suggesting a contribution from the encapsulated HRP.

Considering that encapsulation is a statistic process, multiple species should be present, including such species as empty PS–PIAT and empty ABA nanoreactors. To probe the existence of these species and their contribution to the cascade process, we stained the inner compartment by a reaction commonly used in histochemistry, the so-called catalyzed reporter deposition.[43] This reaction makes use of the HRP-catalyzed oxidation of tyramides into radicals, which rapidly react with electron-rich amino acid moieties, mostly tyrosines (for reaction see ESI Fig. S7†). The use of tyramides carrying a fluorescent label leads to fluorescent staining. In our case, successful staining would show that HRP is active in the OmpF-equipped MCPs, while concomitant fluorescent labeling of GOx would show colocalization of the fluorescent signals.

Following this strategy, we prepared MCPs containing alexa-488 labeled GOx. We then incubated these MCPs with tyramide alexa-647, and subsequently removed the dye by overnight dialysis. Investigating the MCPs by confocal microscopy showed a fluorescence signal at 488 nm for MCPs with and without OmpF, showing the successful encapsulation of labeled GOx (Fig. 3a, b and S9a, b†). Importantly, when visualizing the structures in the red channel, an intense signal was observed for the MCP with OmpF embedded in the inner compartment's membrane, while this signal was absent in the control

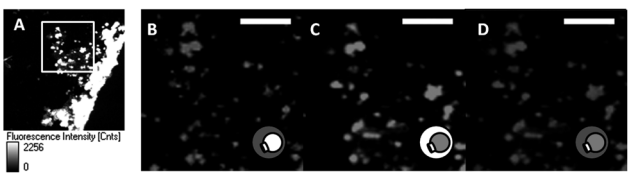

Fig. 3 Confocal microscope imaging of MCPs with OmpF embedded in the inner compartment. MCPs were prepared as described above. GOx was labeled with alexa-488 and imaged in the blue channel (a and b; where b is the magnification of a, as indicated by the white square). After preparation of the MCPs, HRP was stained by its reaction with alexa-647 tyramide and imaged in the red channel. (c) Fluorescence in the red channel was only observed when the OmpF channel was present in the inner compartment's membrane (compare c and Fig. S9c†). (d) Composite image of the blue and red channels, showing the co-localization of the labels, which implies that the reaction takes place in the same structure. Scale bars are 20 μm. For the respective images of the blank sample (*i.e.*, with closed compartments), see Fig. S9.†

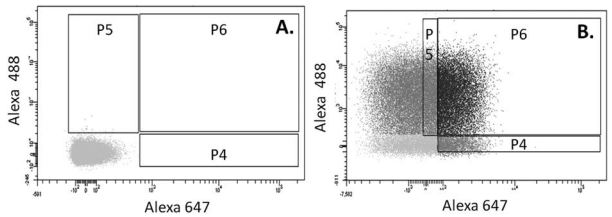

Fig. 4 Flow cytometry analysis of MCPs. (a) MCPs before labeling of GOx and HRP. No fluorescence is observed in the sample. (b) MCPs after labeling GOx and HRP with alexa-488 and alexa-674, respectively. Note that HRP has been labeled by tyramide staining so that only active HRP is visible. Gates P4 and P5 indicate labeled ABA polymersomes (red, as judged from the fluorescence of the HRP) and labeled PS–PIAT polymersomes (green), respectively, while gate P6 indicates double-labeled polymersomes, *i.e.*, MCPs.

containing the 'closed' compartments (compare Fig. 3c and S9c†). This confirmed that only when OmpF is present, the dye diffuses into the inner compartment where it is subsequently transformed by HRP. Comparison of the signals at both wavelengths shows that the fluorescent signals at different wavelengths are co-localized, strengthening the conclusion that a considerable fraction of enzymes is encapsulated within a single multicompartment structure (Fig. 3d).

To probe the distribution of the enzymes in the MCPs further, we also subjected the labeled MCPs to flow cytometry (Fig. 4a, b and S10†).[44] These measurements indicated that out of the full population of polymersomes, 28% contained both alexa-647 labeled HRP and alexa-488 labeled GOx (*i.e.*, MCPs), while 5.7% and 16.2% contained alexa-647 labeled HRP (*i.e.*, ABA polymersomes) and alexa-488 labeled GOx (*i.e.*, PS–PIAT polymersomes), respectively. In other words, assuming most GOx to be labeled, this suggests that, upon addition of PS–PIAT, 44.2% of the resulting polymersome population carried GOx, of which the majority (63%) also contained (active) HRP (Table S2†). Considering the ABA nanoreactors, an even higher fraction of the total ABA population appeared to coexist with PS–PIAT (83%), which is attributed to the filtration process, leading to disintegration of the single ABA nanoreactors. Considering that only active enzymes were detected, this thus suggests that most of the cascade activity results from the MCPs.

Conclusions

In conclusion, we have shown the construction of a multicompartment polymersome structure where we employed the passive protein channel OmpF, embedded into the inner membrane, to allow for the exchange of molecules. Selective encapsulation of GOx in the outer compartment and HRP in the inner compartment resulted in an efficient enzymatic cascade system only when OmpF was embedded in the inner compartment's membrane. The demonstration of a multicompartment structure functionalized with membrane proteins forms a new step in the mimicry of the compartmentalization of cells, and allows us to tap into the selectivity displayed by such membranes, opening the possibility of engineering truly specialized multicompartment polymersomes.

Acknowledgements

The authors would like to acknowledge Mahendra Yavvari for experimental assistance, Fu Zhikang for flow cytometry measurements, Dr Law Jia Yan for TEM measurements, and Patric Baumann for preparing samples for cryo-TEM. We thank Prof. Subbu Venkatraman's team for light scattering measurements. The electron microscopy work was performed at the Facility for Analysis, Characterization, Testing, and Simulation (FACTS) in Nanyang Technological University, Singapore.

Notes and references

1 B. Alberts, A. Johnson, J. Lewis, M. Raff, K. Roberts and P. Walter, *Molecular Biology of the Cell*, Garland Science, New York, 4th edn, 2002, pp. 3–12.
2 J. W. Szostak, D. P. Bartel and P. L. Luisi, *Nature*, 2001, **409**, 387–390.
3 M. Delcea, A. Yashchenok, K. Videnova, O. Kreft, H. Möhwald and A. G. Skirtach, *Macromol. Biosci.*, 2010, **10**, 465–474.
4 C. M. Paleos and D. Tsiourvas, *J. Mol. Recognit.*, 2006, **19**, 60–67.
5 R. Chandrawati, M. P. van Koeverden, H. Lomas and F. J. Caruso, *J. Phys. Chem. Lett.*, 2011, **2**, 2639–2649.
6 H. C. Chiu, Y. W. Lin, Y. F. Huang, C. K. Chuang and C. S. Chern, *Angew. Chem., Int. Ed.*, 2008, **47**, 1875–1878.
7 H. M. de Hoog, M. Nallani and N. Tomczak, *Soft Matter*, 2012, **8**, 4552–4561.
8 T. Hamada, Y. Miura, K. Ishii, S. Araki, K. Yoshikawa, M. Vestergaard and M. Takagi, *J. Phys. Chem. B*, 2007, **111**, 10853–10857.
9 N. P. Kamat, J. S. Katz and D. A. Hammer, *J. Phys. Chem. Lett.*, 2011, **2**, 1612–1623.
10 O. Kreft, M. Prevot, H. Möhwald and G. B. Sukhorukov, *Angew. Chem., Int. Ed.*, 2007, **46**, 5605–5608.
11 M. S. Long, A. S. Cans and C. D. Keating, *J. Am. Chem. Soc.*, 2008, **130**, 756–762.
12 M. Marguet, L. Edembe and S. Lecommandoux, *Angew. Chem., Int. Ed.*, 2012, **51**, 1173–1176.
13 B. Stadler, R. Chandrawati, A. D. Price, S.-F. Chong, K. Breheney, A. Postma, L. A. Connal, A. N. Zelikin and F. Caruso, *Angew. Chem., Int. Ed.*, 2009, **48**, 4359–4362.
14 P. Y. Bolinger, D. Stamou and H. Vogel, *J. Am. Chem. Soc.*, 2004, **126**, 8594–8595.
15 C. Boyer and J. A. Zasadzinski, *ACS Nano*, 2007, **1**, 176–182.
16 S. A. Walker, M. T. Kennedy and J. A. Zasadzinski, *Nature*, 1997, **387**, 61–64.
17 J. A. Zasadzinski, B. Wong, N. Forbes, G. Braun and G. Wu, *Curr. Opin. Colloid Interface Sci.*, 2011, **16**, 203–214.
18 G. Decher, *Science*, 1997, **277**, 1232–1237.
19 B. M. Discher, Y.-Y. Won, D. S. Ege, J. C.-M. Lee, F. S. Bates, D. E. Discher and D. A. Hammer, *Science*, 1999, **284**, 1143–1146.
20 D. E. Discher and A. Eisenberg, *Science*, 2002, **297**, 967–973.
21 K. T. Kim, S. A. Meeuwissen, R. J. M. Nolte and J. C. M. van Hest, *Nanoscale*, 2010, **2**, 844–858.

22 S. F. M. van Dongen, M. Nallani, J. J. L. M. Cornelissen, R. J. M. Nolte and J. C. M. van Hest, *Chem. – Eur. J.*, 2009, **15**, 1107–1114.
23 A. Graff, M. Sauer, P. van Gelder and W. Meier, *Proc. Natl. Acad. Sci. U. S. A.*, 2002, **99**, 5064–5068.
24 M. Kumar, M. Grzelakowski, J. Zilles, M. Clark and W. Meier, *Proc. Natl. Acad. Sci. U. S. A.*, 2007, **104**, 20719–20724.
25 W. Meier, C. Nardin and M. Winterhalter, *Angew. Chem., Int. Ed.*, 2000, **39**, 4599–4602.
26 M. Nallani, O. Onaca, N. Gera, K. Hildenbrand, W. Hoseisel and U. Schwaneberg, *Biotechnol. J.*, 2006, **1**, 828–834.
27 C. Nardin, S. Thoeni, J. Widmer, M. Winterhalter and W. Meier, *Chem. Commun.*, 2000, 1433–1434.
28 Z. Fu, M. Andreasson-Ochsner, H.-P. M. de Hoog, N. Tomczak and M. Nallani, *Chem. Commun.*, 2011, **47**, 2862–2864.
29 L. Hosta-Rigau, *Adv. Funct. Mater.*, 2010, **20**, 59–66.
30 H. C. Shum, Y. J. Zhao, S. H. Kim and D. A. Weitz, *Angew. Chem., Int. Ed.*, 2011, **50**, 1648–1651.
31 K. Kita-Tokarczyk, J. Grumelard, T. Haefele and W. Meier, *Polymer*, 2005, **46**, 3540–3563.
32 S. May, M. Andreasson-Ochsner, Z. Fu, Y. X. Low, D. Tan, H.-P. M. de Hoog, S. Ritz, M. Nallani and E.-K. Sinner, *Angew. Chem., Int. Ed.*, 2013, **52**, 749–753.
33 M. Nallani, M. Andreasson-Ochsner, C.-W. D. Tan, E.-K. Sinner, Y. Wisantoso, S. Geifman-Shochat and W. Hunziker, *Biointerphases*, 2011, **6**, 153–157.
34 M. Andreasson-Ochsner, Z. Fu, S. May, L. Y. Xiu, M. Nallani and E.-K. Sinner, *Langmuir*, 2012, **28**, 2044–2048.
35 S. F. M. van Dongen, H.-P. M. de Hoog, R. J. R. W. Peters, M. Nallani, R. J. M. Nolte and J. C. M. van Hest, *Chem. Rev.*, 2009, **109**, 6212–6274.
36 M. Spulber, A. Najer, K. Winkelbach, O. Glaied, M. Waser, U. Pieles, W. Meier and N. Bruns, *J. Am. Chem. Soc.*, 2013, **135**, 9204–9212.
37 C. Nardin, T. Hirt, J. Leukel and W. Meier, *Langmuir*, 2000, **16**, 1035–1041.
38 O. Onaca, P. Sarkar, D. Roccatano, T. Friedrich, B. Hauer, M. Grzelakowski, A. Guven, M. Fioroni and U. Schwaneberg, *Angew. Chem., Int. Ed.*, 2008, **37**, 7029–7031.
39 G. C. Berry, *J. Chem. Phys.*, 1966, **44**, 4550–4564.
40 F. V. D. Velde, F. V. Rantwijk and R. A. Sheldon, *Trends Biotechnol.*, 2001, **19**, 73–80.
41 H. M. De Hoog, M. Nallani, J. J. L. M. Cornelissen, A. E. Rowan, R. J. M. Nolte and I. W. C. E. Arends, *Org. Biomol. Chem.*, 2009, **7**, 4604–4610.
42 L. Fruk, J. Müller and C. M. Niemeyer, *Chem. – Eur. J.*, 2006, **12**, 7448–7457.
43 M. N. Bobrow, T. D. Harris, K. J. Shaughnessy and G. J. Litt, *J. Immunol. Methods*, 1989, **125**, 279–285.
44 M. Nallani, R. Woestenenk, H.-P. M. de Hoog, S. F. M. van Dongen, J. Boezeman, J. J. L. M. Cornelissen, R. J. M. Nolte and J. C. M. van Hest, *Small*, 2009, **5**, 1138–1143.